offers high separation efficiencies (up to $\sim 10^6$ theoretical plates) and can be performed in capillary structures capable of handling sample volumes in the low femtoliter range, the on-line analysis with CE patch-clamp detection of evoked neurotransmitter release from biological microenvironments such as single cells or discrete nerve terminal areas should be feasible because sample integrity is conserved.

REFERENCES AND NOTES

1. L. E. Rabow *et al.*, *Synapse* **21**, 189 (1995).
2. C. E. Jahr and R. A. Lester, *Curr. Opin. Neurobiol.* **2**, 270 (1992).
3. C. J. McBain and M. L. Mayer, *Physiol. Rev.* **74**, 723 (1994).
4. G. A. Rechnitz, T. L. Riechel, R. K. Kobos, M. E. Meyerhoff, *Science* **199**, 440 (1978); R. M. Buch and G. A. Rechnitz, *Anal. Chem.* **61**, 533A (1989); H. M. McConnell *et al.*, *Science* **257**, 1906 (1992); Y. Hu *et al.*, *Brain Res.* **659**, 117 (1994); W. S. Leal *et al.*, *Proc. Natl. Acad. Sci. U.S.A.* **92**, 1033 (1995); *ibid.*, p. 1038.
5. R. I. Hume, L. W. Role, G. D. Fischbach, *Nature* **305**, 632 (1983); S. H. Young and Mu-ming Poo, *ibid.*, p. 634.
6. D. R. Copenhagen and C. E. Jahr, *ibid.* **341**, 536 (1989); T. Maeda *et al.*, *Neuron* **15**, 253 (1995).
7. E. Neher and B. Sakmann, *Nature* **260**, 799 (1976); O. P. Hamill *et al.*, *Pfluegers Arch.* **391**, 85 (1981); B. Sakmann and E. Neher, *Single-Channel Recording* (Plenum, New York, ed. 2, 1995).
8. Even if Glu most likely is the main neurotransmitter acting on NMDA receptors at brain synapses [(2); (24); R. A. Lester and C. E. Jahr, *J. Neurosci.* **12**, 635 (1992)], numerous compounds endogenous to the mammalian brain are known to activate this receptor [(24); X. Li *et al.*, *Neurosci. Lett.* **155**, 42 (1993); P. Q. Trombley and G. L. Westbrook, *J. Neurophysiol.* **64**, 598 (1990)] and to be released by K^+ in a Ca^{2+}-dependent manner [K. Q. Do *et al.*, *J. Neurochem.* **46**, 779 (1986); M. Zollinger *et al.*, *ibid.* **63**, 1133 (1994); M. Kimura *et al.*, *Neuroscience* **66**, 609 (1995)]. Extracellular overflow of NMDA receptor agonists has also been observed during episodes of cerebral ischemia, anoxia, and hypoglycemia [D. W. Choi, *Neuron* **1**, 623 (1988); B. Meldrum, in *Diversity of Interacting Receptors*, L. G. Abood and A. Lajtha, Eds. (New York Academy of Sciences, New York, 1995), vol. 757, pp. 492–505; H. Hagberg *et al.*, *J. Cerebral Blood Flow Metab.* **5**, 413 (1985); M. Sandberg *et al.*, *J. Neurochem.* **47**, 178 (1986); P. Andiné *et al.*, *ibid.* **57**, 230 (1991); O. Orwar *et al.*, *ibid.* **63**, 1371 (1994)]. Furthermore, unnatural NMDA receptor agonists are important for the etiology of some neurodegenerative diseases [J. W. Olney *et al.*, *J. Neuropathol. Exp. Neurol.* **34**, 167 (1975); P. S. Spencer *et al.*, *Science* **237**, 517 (1987); J. H. Weiss and D. W. Choi, *ibid.* **241**, 973 (1988)]. Also, the chemical nature of the coagonist acting on NMDA receptors is not firmly established [S. Cull-Candy, *Curr. Biol.* **5**, 841 (1995)].
9. J. B. Shear *et al.*, *Science* **267**, 74 (1995).
10. H. A. Fishman *et al.*, *Proc. Natl. Acad. Sci. U.S.A.* **92**, 7877 (1995).
11. I. Jacobson, *Neurosci. Res. Commun.* **8**, 11 (1991); _____ and X. Li, *ibid.* **10**, 177 (1992).
12. P. Q. Trombley and G. M. Shepherd, *Curr. Opin. Neurobiol.* **3**, 540 (1993); *J. Neurophysiol.* **71**, 761 (1994).
13. The CE separations were performed in fused-silica capillaries 50 μm in inner diameter (50 cm long) with a high-power supply operated at 12 kV. The inlet end of the capillary was positioned 10 cm above the outlet end. In the sample injections we placed the capillary inlet in sample solution 20 cm above the outlet end for 10 s. The fractured part of the separation capillary was enclosed in a 1-ml polyethylene vial filled with Hepes-saline solution and connected to ground by a Pt wire. We compensated for residual potentials resulting from incomplete grounding by applying a patch-clamp offset potential.
14. Patch pipettes were fabricated from thick-walled borosilicate glass and had tip diameters of ~2 μm (resistance, 5 to 15 megohms; series resistance, <50 megohms). The pipette shanks were treated with Sigmacote (Sigma, St. Louis, MO) and filled with a solution containing 140 mM CsCl, 2 mM $MgCl_2$, 1 mM $CaCl_2$, 11 mM EGTA, and 10 mM Hepes; the pH was adjusted to 7.2 with KOH. Both the outside-out patch-clamp and the whole-cell patch-clamp recording configurations were used, as specified in the text. For outside-out patch-clamp experiments, cells were plated onto cover slips treated with poly-L-lysine and allowed to adhere to the surface for 1 hour before recording. The signals were recorded with a List L/M EPC-7 amplifier, digitized (20 kHz, PCM 2 A/D VCR adapter), and stored on video tape. Data acquisition and initial analysis were performed with programs supplied by J. Dempster, University of Strathclyde, United Kingdom.
15. R. A. Wallingford and A. G. Ewing, *Anal. Chem.* **59**, 1762 (1987).
16. B. Katz and R. Miledi, *J. Physiol. (London)* **224**, 665 (1972); C. R. Anderson and C. F. Stevens, *ibid.* **235**, 655 (1973); D. Colquhoun and A. G. Hawkes, *Proc. R. Soc. London Ser. B* **199**, 231 (1977).
17. The signals from the video tape were low-pass–filtered (1 kHz, −3 dB, 8-pole Butterworth filter) and digitized at 2 kHz. Current records were divided into 0.5-s blocks, and we calculated the power spectra by averaging at least 20 blocks. The resulting spectra were fitted to the sum of two Lorentzian functions:

$$G(f) = \Sigma S(0)_i/[1 + (f/f_{ci})^2]$$

where $G(f)$ is the spectral density, $S(0)_i$ is the low-frequency asymptote of the ith component, f is the frequency, and f_{ci} is the corner frequency (half-amplitude) of the ith component. Curve-fitting was performed with a least squares Levenberg-Marquart algorithm that used proportional weighting. Current traces were used only if the mean current was stable. Apparent single-channel conductances were estimated from

$$\gamma = \sigma^2/[I_m(V - V_{eq})]$$

where σ^2 is the current variance, I_m is the mean current, V is the holding potential (−70 mV), and V_{eq} is the reversal potential (assumed to be 0 mV).
18. M. Kaneda *et al.*, *J. Physiol. (London)* **485**, 419 (1995).
19. P. Ascher, P. Bregestovski, L. Nowak, *ibid.* **399**, 207 (1988).
20. J. Bufler *et al.*, *J. Comp. Physiol. A* **170**, 153 (1992); G. Kilic *et al.*, *Eur. J. Neurosci.* **5**, 65 (1993); B. Schönrock and J. Bormann, *ibid.*, p. 1042.
21. O. Orwar *et al.*, data not shown.
22. C. E. Jahr and C. F. Stevens, *Nature* **325**, 522 (1987); S. G. Cull-Candy and M. M. Usowicz, *ibid.*, p. 525; J. R. Howe *et al.*, *J. Physiol. (London)* **432**, 143 (1991).
23. G. H. Ma *et al.*, *Mol. Pharmacol.* **47**, 1035 (1995).
24. D. K. Patneau and M. L. Mayer, *J. Neurosci.* **10**, 2385 (1990).

25. Helpful discussions with A. Hamberger, M. Sandberg, S. G. Weber, M. E. Meyerhoff, and D. T. Chiu and technical assistance from H. Zhao and R. Dadoo are gratefully acknowledged. This work was supported by grants from the National Institute of Mental Health (MH 45423-06) and the National Institute of Drug Abuse (DA 09873-01). The work of O.O. was supported by the Swedish Natural Science Research Council (K-PD 10481-303), and that of A.M. was supported by the German Gottlieb Daimler- and Karl Benz-Foundation (2.95.32).

1 February 1996; accepted 3 April 1996

Nanoscale Magnetic Domains in Mesoscopic Magnets

Michel Hehn, Kamel Ounadjela,* Jean-Pierre Bucher, Françoise Rousseaux, Dominique Decanini, Bernard Bartenlian, Claude Chappert

The basic magnetic properties of three-dimensional nanostructured materials can be drastically different from those of a continuous film. High-resolution magnetic force microscopy studies of magnetic submicrometer-sized cobalt dots with geometrical dimensions comparable to the width of magnetic domains reveal a variety of intricate domain patterns controlled by the details of the dot geometry. By changing the thickness of the dots, the width of the geometrically constrained magnetic domains can be tuned. Concentric rings and spirals with vortex configurations have been stabilized, with particular incidence in the magnetization reversal process as observed in the ensemble-averaged hysteresis loops.

Mesoscopic magnets are currently being studied for their fundamental and technological properties. These magnets are found in several forms: as particles or patterned submicrometer-sized dots in close interaction with a substrate (*1*–*5*) or as free atomic clusters in beams (*5*, *6*). Very small monodomain Co particles (a few tens of atoms) do not show any hysteretic behavior at room temperature (*6*), whereas in bigger particles, which are relevant to high-density data storage materials, anisotropies build up that lock the magnetic moment in a given direction. Interesting properties are expected as the geometrical dimensions of the particles become comparable to character-

M. Hehn, K. Ounadjela, J.-P. Bucher, Institut de Physique et Chimie des Matériaux de Strasbourg, 23 rue du Loess, 67037 Strasbourg Cedex, France.
F. Rousseaux and D. Decanini, L2M/CNRS, 196 Avenue Henri Ravera, 92225 Bagneux, France.
B. Bartenlian and C. Chappert, Institut d'Electronique Fondamentale, Université Paris-Sud, 91405 Orsay Cedex, France.
*To whom correspondence should be addressed.

istic nanoscopic length scales such as the magnetic exchange length and mesoscopic dimensions such as domain width (*7*).

In order to study static and dynamic magnetism in very small particles with diameters of tens to hundreds of nanometers, one can either study one particle at a time with a local technique such as a superconducting quantum interference device (SQUID) loop surrounding the particle to be studied (*8*) or perform average magnetic measurements on assemblies of many identical (monodisperse, similarly shaped) dots (*1*, *2*, *4*). The latter approach has been adopted by several groups, and reliable x-ray (*9*), electron beam (*10*, *11*), and scanning tunneling microscopy–assisted (*2*) techniques have been developed to synthesize large arrays of identical dots, in which the magnitude of the interaction between the particles can be tuned by varying the period of the array. Magnetic domain configurations and reversal processes that have been extensively studied since the turn of the century now had to be reexamined for nanostructured materials (*12*).

We focused on submicrometer-sized Co dots, magnetized perpendicular to the plane of the array. The dots were patterned by x-ray photolithography in single crystalline Co films and contained several magnetic domains whose sizes we could tune by adjusting the thickness of the film (*13*). Effects of the boundaries then became apparent, and the domain geometry was found to be strongly dependent on the aspect ratio (the ratio of the height to the length of the dots). The film properties before the photolithographic process were compared with the properties of the dot arrays. We used conventional magnetometry to characterize the overall magnetic properties of a large number of identical dots. The domain structure of individual particles was studied by local magnetic force microscopy (MFM).

Arrays of square dots 5 by 5 mm^2 with a lateral dimension of 0.5 μm and a lattice periodicity of 1 μm were patterned from epitaxial Co films grown in ultrahigh vacuum with thicknesses, t_{Co}, varying from 10 to 150 nm (Fig. 1). Before the Co deposition, a 20-nm-thick Ru buffer layer was grown onto an Al_2O_3(1,1,-2,0) sapphire substrate; the Co layer was subsequently grown and capped by 5-nm Ru. The high crystalline quality of the hexagonal close-packed (hcp) (0001) phase of the Co films was confirmed by in situ and ex situ techniques (*14*). We patterned the films by x-ray lithography and ion-beam etching, using a soft technique developed earlier to avoid the deterioration of fragile multilayered samples (*9*).

We performed magnetization measurements for all samples at room temperature,

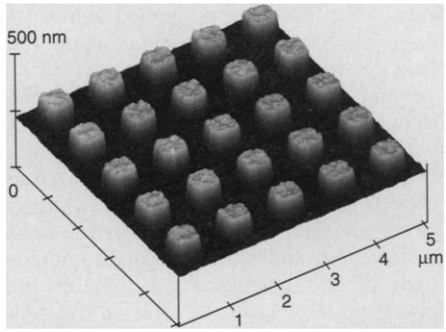

Fig. 1. Oblique view of a 25-nm-thick Co dot array obtained with an atomic force microscope. The lateral size of the dot is 0.5 μm, and the lattice periodicity is 1 μm. The edges are straight with nearly a vertical profile, and the surfaces of the dots have retained the smoothness observed on the as-grown films. This quality of patterning was retained for Co films up to 150 nm thick.

using an alternating gradient force magnetometer with the field applied perpendicular and parallel to the film plane. The magnetization curves for a 100-nm-thick film and for the same film patterned into an array of dots (Fig. 2), with the field applied perpendicular to the substrate, are reminiscent of perpendicularly magnetized multidomain structures (*15*). The singularity at H_n in the magnetization versus field curve of Fig. 2 is ascribed to a nucleation of magnetic bubbles in an otherwise saturated environment (all magnetic moments oriented along the field direction). The linear variation at smaller fields is due to irreversible magnetic wall motion. Differences between arrays and films appear in both the nucleation field H_n and the saturation field H_s (Fig. 2). Instead of increasing with thickness up to $4\pi M_s$ (where M_s is the saturation magnetization) as in continuous films, both of these fields decrease as the dot thickness is increased.

In MFM, the resolution is solely limited by the distance at which the tip is scanned above the surface and by the tip radius, typically 50 nm. A Nanoscope III, equipped with a CoCr-coated Si tip magnetized along the tip axis, was used in the vibrating-lift mode developed by Digital Instruments. The detected signal (frequency shift of the vibrating cantilever) is proportional to the second derivative of the local field, and therefore this technique provides a good signal-to-noise ratio. For domain sizes under consideration here, we have shown that MFM contrasts can be identified unequivocally with mainly "up" and "down" perpendicularly oriented domains (*14*). Before the MFM measurements, the samples were either magnetized or demagnetized in fields perpendicular or parallel to the film plane. During the demagnetization processes, we swept the field alternately from positive to

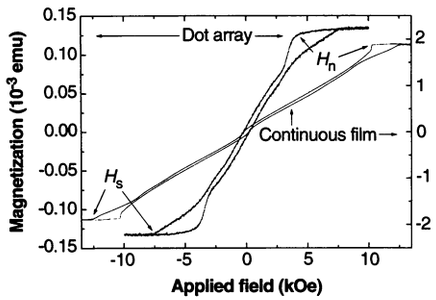

Fig. 2. Perpendicular magnetization curves for both film and arrays with the external field applied perpendicular to the film plane. The thickness of the Co film and array is 100 nm; emu, electromagnetic unit.

negative values while simultaneously reducing the field amplitude. For perpendicular or parallel magnetization, the field was abruptly turned off after saturation.

Two parameters can be used to consider the effects of geometry: (i) the dot height, which determines the domain size in much the same way as film thickness does in the case of infinite films, and (ii) the dot shape, determined primarily by the aspect ratio, which induces the particular pattern of the domain structure. In this work, the square base of the dot was kept constant (0.5 μm by 0.5 μm) and the aspect ratio was varied from 0.05 for t_{Co} = 25 nm to 0.3 for t_{Co} = 150 nm. When the domain size is much smaller than the base of the dot, the magnetostatic energy at any point inside a dot is determined primarily by nearby domains, although the dipolar interaction is a long-range interaction. Therefore, identical stripe periods are expected for a continuous film and for dot arrays. Shape effects, by contrast, dominate the orientation of domains in the dots and distinguish patterned array behavior from continuous film behavior.

The domain configurations in the perpendicular remnant state consist of magnetic bubbles (Fig. 3, A and C). A predominantly single bubble configuration is seen for the 150-nm-thick dot array (Fig. 3A), although the precision of the MFM experiment is not sufficient to exclude the presence of small domains or nonuniform "flower" states at the dot edges (*16*). The circular bubble is nucleated at the center of the dot where the demagnetizing field is the highest and does not grow bigger as a result of the repulsive interactions with the edges. The space available within each dot is just sufficient to accommodate one single bubble. The domain structure observed in the 50-nm-thick dots array (Fig. 3C) consists of a metastable network of bubbles, similar to the bubble array found in the continuous film with the same thickness (*14*). After perpendicular demagnetization, the domain

patterns consisted of bubbles and randomly oriented stripe-like domains (Fig. 3, B and D). The domains of the 150-nm-thick dots look like dumbbell patterns (Fig. 3B), resulting probably from elliptical distortion and elongation of the one single nucleated domain (*17*), whereas the domains of the 50-nm-thick dots reveal disclination instabilities (Fig. 3D) related to the conservation of the in-plane symmetry (*17*).

The stripe orientation is very sensitive to the direction of the in-plane component of the applied field (Fig. 4). For the 50-nm-thick Co dots (Fig. 4, C and D), the stripe direction is aligned with the in-plane magnetic field component applied before the MFM measurements. The tendency of the domain walls to avoid the edges of the dot and of the domains to increase their length is clearly apparent in the case of an in-plane demagnetization along the diagonal of the array. This tendency results from the geometrical constraints and is enhanced when the dot height is reduced (see Fig. 4, E and F, for results from a 25-nm-thick dot array). In this instance, the domain pattern consists of spirals or concentric cylinders of alternate magnetization irrespective of the direction of the applied field. The 150-nm-thick dot array (Fig. 4, A and B) presents an interesting limiting case in which the width of the domain becomes comparable to the lateral size of the dot. Although the shape of the domain patterns is similar to that of dumbbells, the preferential diagonal direction along which they orient depends on the direction of the applied field. If the field is applied parallel to the side of a dot, the domains reorient ±45° away from the direction of the demagnetization field. However, when the field is applied along the diagonal, the domains remain along the field direction.

Simple arguments can account for the formation of domains during in-plane demagnetization. As the dot is exposed to a large enough in-plane magnetic field, one expects all magnetic moments to align along the field direction. When the field is decreased and while the main component of the magnetization remains in-plane, vortices begin to form at the corners of the dots to reduce the in-plane demagnetizing field (*18*). The system minimizes the exchange energy by having the magnetization at the center of the vortex perpendicular to the surface. During the field decrease the magnetization rotates coherently out-of-plane; this results in a magnetization perpendicular to the film with regions (where vortices were created, that is, mostly at corners) that have opposite magnetization.

When the bubble diameter is comparable to the lateral dimensions of the dot (as for the 150-nm-thick dot array), only two bubbles nucleate at opposite corners; this reduces their dipolar interaction, and the bubbles partly coalesce to form dumbbell-shaped domains because of their large diameter (Fig. 4, A and B). For symmetry reasons, when the field is applied along the side of a dot, the dumbbells align either along one diagonal or the other (Fig. 4A). When the bubble diameter is small compared to the lateral dimensions of the dot (as for the 50-nm-thick dot array), the bubble nucleated at the edge remains pinned on it but can run out into stripes (Fig. 4, C and D). Although the domain structures never look exactly the same from one dot to the next, their energies are very close because they are for the most part reproducible mirror images of each other.

The high geometrical quality of the dots is reflected in the concentric ring configurations obtained after parallel demagnetization of 25-nm-thick dots (Fig. 4, E and F). At this reduced dot thickness, the energy is smallest for in-plane magnetic moments. The main component of the magnetization therefore remains in-plane and parallel to the edges of the dots, which results in a circular domain structure with a singularity at the center of the dot where the in-plane magnetization reorients fully perpendicular to form a vortex. The concentric ring structure observed in the MFM images is due to small, alternately up and down, perpendicular components also observed in the stripe structure of hcp Co films (*14*, *19*).

How domain confinement proceeds in the 25-nm-thick Co dot array is particularly interesting. The curve of the first perpendicular magnetization (Fig. 5), taken after the sample had undergone in-plane demagnetization, displays one pronounced jump of the magnetization which occurs within a field interval of 2 0e. The dipolar interaction between dots is so weak that no collective behavior can be invoked to explain this phenomenon, and thus the observation of the simultaneous switching of millions of dots necessarily implies that the collapse field is most sensitive to local parameters such as the thickness and quality of the

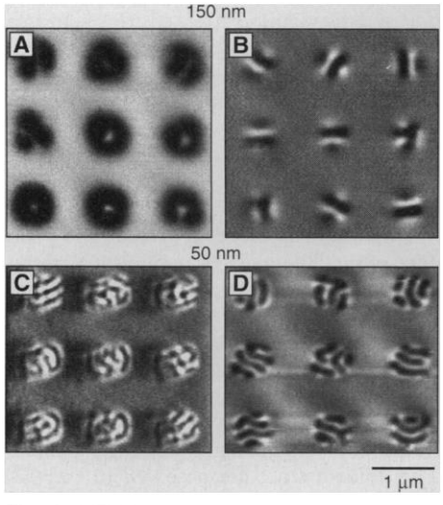

Fig. 3. MFM images in zero applied field after perpendicular saturation for (**A**) 150-nm-thick and (**C**) 50-nm-thick Co dot arrays and after perpendicular demagnetization for (**B**) 150-nm-thick and (**D**) 50-nm-thick Co dot arrays.

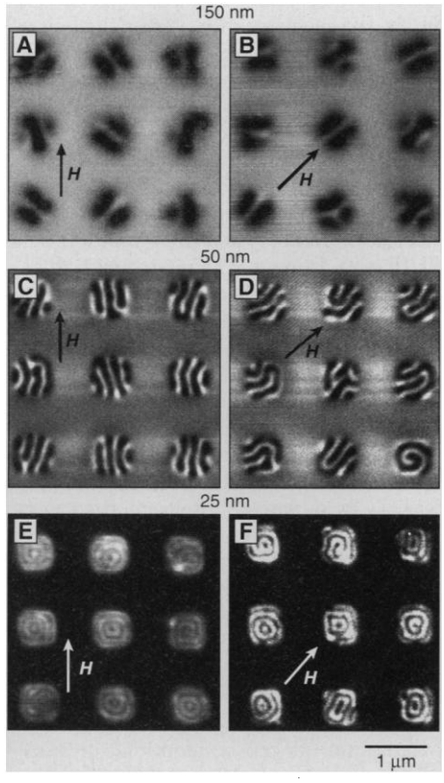

Fig. 4. MFM images in zero applied field after parallel demagnetization along the side of the dot for (**A**) 150-nm-thick, (**C**) 50-nm-thick, and (**E**) 25-nm-thick Co dot arrays and after parallel demagnetization along the diagonal of the dot for (**B**) 150-nm-thick (**D**), 50-nm-thick, and (**F**) 25-nm-thick Co dot arrays.

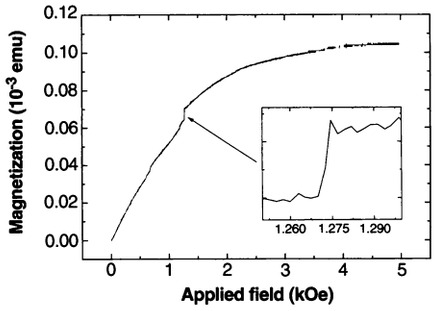

Fig. 5. First perpendicular magnetization curve for the 25-nm-thick Co dot array. (**Inset**) A close-up of the region where the jump occurs and gives evidence of the field transition within 2 Oe.

material, in principle identical over the whole sample surface. We attribute this singularity, which corresponds to about 6% of the magnetization at saturation, to the collapse of the central domain in roughly half of the dots oriented antiparallel to the field direction. This switching field is expected to be most sensitive to the local parameters of the material and less sensitive to the finite size and shape of the dots. This result is due to a combination of the central position of the domain, which is far away from the edges, and the presence of the nearby alternately oriented magnetic domains, which ensure efficient screening of the edges. Close examination of the magnetization curve (Fig. 5) reveals at least two more, although weaker, jumps at lower field (reproducible under identical conditions) that can be attributed to the initial collapse of part of the outer rings. Such a distribution of jumps may result because the height of one jump depends on both the size of the domain to be reversed and the number of dots with the same configuration. Not surprisingly, after the dots have become single-domain, a further increase in the field is necessary to overcome the strong demagnetizing field near the bottoms and the tops of the dots and to completely align the moments along the field direction.

Our results demonstrate that two length scales determine the magnetic domain structures and magnetic domain reversal processes in Co dot arrays. One length scale is set by the geometry of the dots, and the other is imposed by the size of a domain wall separating two adjacent domains. When starting from a previously stabilized concentric ring configuration, we observe clear jumps in the first magnetization curve of an array that are clearly linked to specific domain annihilation processes.

Investigating domain patterns in magnetic storage devices is becoming increasingly necessary for industrial applications as written bits become smaller and smaller. In order to prevent accidental switching of magnetic domains, stringent control of the quality of the material and the dot geometry is required.

REFERENCES AND NOTES

1. G. A. Gibson and S. Schultz, *J. Appl. Phys.* **73**, 4516 (1993).
2. A. D. Kent, S. von Molnar, S. Gider, D. D. Awschalom, *ibid.* **76**, 6656 (1994).
3. J. Shi *et al.*, *Nature* **377**, 707 (1995).
4. S. Manalis *et al.*, *Appl. Phys. Lett.* **66**, 2585 (1995).
5. J. Shi, S. Gider, K. Babcock, D. D. Awschalom, *Science* **271**, 937 (1996).
6. J. P. Bucher and L. A. Bloomfield, *Int. J. Mod. Phys.* **7**, 1079 (1993).
7. *Phys. Today* **48** (1995).
8. W. Wernsdorfer *et al.*, *J. Magn. Magn. Mater.* **145**, 33 (1995).
9. F. Rousseaux *et al.*, *J. Vac. Sci. Technol. B* **13**, 2787 (1995).
10. R. M. H. New, R. F. W. Pease, R. L. White, *ibid.* **12**, 3196 (1994).
11. P. R. Krauss, P. B. Fischer, S. Y. Chou, *ibid.*, p. 3639.
12. D. R. Fredkin, T. R. Koehler, J. F. Smyth, S. Schultz, *J. Appl. Phys.* **69**, 5276 (1991).
13. The width of the domains is proportional to the square root of the thickness of the film as predicted by C. Kittel in *Phys. Rev.* **70**, 965 (1946).
14. M. Hehn, S. Padovani, K. Ounadjela, J. P. Bucher, *Phys. Rev. B*, in press.
15. C. Kooy and U. Enz, *Philips Res. Rep.* **15**, 7 (1960).
16. Y. Nakatani, Y. Uesaka, N. Hayashi, *Jpn. J. Appl. Phys.* **28**, 2485 (1989).
17. M. Seul and D. Andelman, *Science* **267**, 476 (1995) and references therein.
18. The mechanism is similar to the one described for Permalloy particles with in-plane magnetization (*12*), where the vortices move toward the center of the dot as the field is further decreased.
19. D. M. Donnet, K. M. Krishnan, Y. Yajima, *J. Phys. D* **28**, 1942 (1995).

20. We thank H. van den Berg, P. Panissod, and R. Stamps for fruitful discussions and J. Arabski, N. Bardou, E. Cambril, F. Carcenac, S. Padovani, and M. F. Ravet for technical support. Supported in part by the European Human Capital and Mobility Program.

1 February 1996; accepted 15 April 1996

Adenosine Diphosphate as an Intracellular Regulator of Insulin Secretion

C. G. Nichols,* S.-L. Shyng, A. Nestorowicz, B. Glaser, J. P. Clement IV, G. Gonzalez, L. Aguilar-Bryan, M. A. Permutt,† J. Bryan†

Adenosine triphosphate (ATP)–sensitive potassium (K_{ATP}) channels couple the cellular metabolic state to electrical activity and are a critical link between blood glucose concentration and pancreatic insulin secretion. A mutation in the second nucleotide-binding fold (NBF2) of the sulfonylurea receptor (SUR) of an individual diagnosed with persistent hyperinsulinemic hypoglycemia of infancy generated K_{ATP} channels that could be opened by diazoxide but not in response to metabolic inhibition. The hamster SUR, containing the analogous mutation, had normal ATP sensitivity, but unlike wild-type channels, inhibition by ATP was not antagonized by adenosine diphosphate (ADP). Additional mutations in NBF2 resulted in the same phenotype, whereas an equivalent mutation in NBF1 showed normal sensitivity to MgADP. Thus, by binding to SUR NBF2 and antagonizing ATP inhibition of K_{ATP} channels, intracellular MgADP may regulate insulin secretion.

Potassium channels that are ATP-sensitive are found in many types of cells and serve to couple metabolic state to electrical activity (*1*). By hyperpolarizing the cell, K_{ATP} channels limit electrical activity and hence reduce calcium entry into muscle and nerve cells. In the pancreas, they are a critical link between blood glucose concentration and insulin secretion (*1*). ATP binding can cause closure of the K_{ATP} channel, and, by antagonizing this action, MgADP causes channel opening. When glucose concentration is low, and hence glycolysis is inhibited, the fall in the intracellular concentration of ATP ([ATP]) and rise in [ADP] may combine to activate pancreatic K_{ATP} channels (*2*, *3*), resulting in hyperpolarization of the β cell, inhibition of calcium entry, and a halt in insulin secretion. The pancreatic K_{ATP} channel is encoded by the sulfonylurea receptor [SUR, a member of the ATP-binding cassette (ABC) superfamily] (*4*) and a small inward rectifier K channel (Kir6.2) subunit (*5*).

If changes in nucleotide concentrations link insulin secretion to the blood glucose concentration, then changes in the ADP or ATP sensitivity of the channel should shift the relation between insulin secretion and blood glucose concentration and lead to either a diabetic, hypoinsulinemic, or hyperinsulinemic state. Inherited mutations in SUR can cause persistent hyperinsulinemic hypoglycemia of infancy (PHHI) (*6*), a disease characterized by glucose-independent insulin secretion (*7*). We isolated mutations in SUR by analysis of genomic DNA samples from individuals affected with PHHI. In one individual, a mutation was found that corresponded to a point mutation (G1479R, where glycine is replaced by arginine at position 1479) in the second nucleotide-binding fold (NBF2) of SUR. The

C. G. Nichols* and S.-L. Shyng, Department of Cell Biology, Washington University School of Medicine, St. Louis, MO 63110, USA.
A. Nestorowicz and M. A. Permutt, Division of Metabolism and Endocrinology, Washington University School of Medicine, St. Louis, MO 63110, USA.
B. Glaser, Division of Endocrinology and Metabolism, Hadassah Medical School, Hebrew University, Jerusalem, Israel.
J. P. Clement IV, G. Gonzalez, L. Aguilar-Bryan, J. Bryan, Departments of Cell Biology and Medicine, Baylor College of Medicine, Houston, TX 77030, USA.

*To whom correspondence should be addressed. E-mail: cnichols@cellbio.wustl.edu
†These authors contributed equally to this work.